TOXICOLOGICAL SCIENCES **133(2)**, 298–308 2013
doi:10.1093/toxsci/kft069
Advance Access publication March 14, 2013

Hydroxyurea Exposure Triggers Tissue-Specific Activation of p38 Mitogen-Activated Protein Kinase Signaling and the DNA Damage Response in Organogenesis-Stage Mouse Embryos

Serena Banh and Barbara F. Hales[1]

Department of Pharmacology and Therapeutics, McGill University, Montreal, QC H3G 1Y6, Canada

[1]To whom correspondence should be addressed at Department of Pharmacology and Therapeutics, McGill University, 3655 Promenade Sir William Osler, Montreal, QC H3G 1Y6, Canada. Fax: (514) 398-7120. E-mail: barbara.hales@mcgill.ca.

Received December 12, 2012; accepted February 28, 2013

Hydroxyurea (HU) is commonly used to treat myeloproliferative diseases and sickle cell anemia. The administration of HU to gestation day 9 CD1 mice causes predominantly hindlimb, tail, and neural tube defects. HU induces oxidative stress and p38 mitogen-activated protein kinase (MAPK) signaling in embryos. HU also inactivates ribonucleotide reductase, leading to DNA replication stress and DNA damage response signaling. We hypothesize that HU exposure induces p38 MAPK activation and DNA damage response signaling during organogenesis preferentially in malformation-sensitive tissues. HU treatment (400 or 600 mg/kg) induced the activation of MEK3/6, upstream MAP2K3 kinases, within 30 min; phospho-MEK3/6 immunoreactivity was increased throughout the embryo. Activation of the downstream p38 MAPK peaked 3 h post-HU treatment. At this time, phospho-p38 MAPK immunoreactivity was enhanced in the cytoplasm and nucleus of cells in the rostral and caudal neuroepithelium and neural tube; significant increases in p38 MAPK signaling were not observed in the somites or heart. Interestingly, the DNA damage response, as assessed by the formation of γH2AX foci, was increased at 3 h in HU-exposed embryos in all tissues examined, including the somites and heart. Increases in pyknotic nuclei and cell fragmentation were observed in all tissues except the heart, an organ that is relatively resistant to HU-induced malformations. Thus, although HU induces a widespread DNA damage response, the activation of p38 MAPK is localized to the rostral and caudal neuroepithelium and neural tube, suggesting that p38 MAPK pathways may play a role in mediating the specific malformations observed after HU exposure.

Key Words: **oxidative stress; replication stress; MAP2K3; MEK3/6; γH2AX; cell death; appendicular skeleton; hindlimb.**

The p38 mitogen-activated protein kinases (MAPKs) (α, β, γ, and δ) are members of a highly conserved superfamily of MAPKs. This family of kinases is of fundamental importance in mediating cellular responses to a wide variety of signals, including cellular stressors such as oxidative stress, UV radiation, cytokines, and DNA damage (She *et al*., 2000; Uhlik *et al*., 2003; Wood *et al*., 2009). In response to stress, p38 MAPKs are activated by phosphorylation on threonine and tyrosine (Thr^{180}/Tyr^{182}) residues within the active site. This phosphorylation is mediated primarily by two upstream dual-specificity kinases, MEK3 and MEK6, that are highly specific for p38 MAPKs (Enslen *et al*., 2000). Activated p38 MAPKs phosphorylate a broad range of substrates both in the cytosol and nucleus. Nuclear shuttling of p38 MAPK has been reported to be triggered specifically by DNA damage inducing stimuli (Wood *et al*., 2009). Substrates of p38 MAPKs include nuclear proteins, such as transcription factors and regulators of chromatin remodeling, and cytosolic proteins implicated in the regulation of cell differentiation and fate (Cuadrado and Nebreda, 2010).

p38 MAPKs play critical roles in numerous biological processes, including cell growth, proliferation, differentiation, death, and cell cycle checkpoints (Deacon *et al*., 2003; Kurosu *et al*., 2005; Puri *et al*., 2000). The role of p38 MAPKs in embryonic development has been investigated extensively in many model organisms, including flies, sea urchins, frogs, and mice. Studies have demonstrated that p38 MAPKs play important roles during oocyte maturation, embryonic cleavage, and axial specification (Bradham and McClay, 2006; Suzanne *et al*., 1999). During murine embryogenesis, the p38 MAPK pathway is essential for skeletogenesis, bone homeostasis, and cardiovascular and placental development (Greenblatt *et al*., 2010; Mudgett *et al*., 2000; Tamura *et al*., 2000). The biological impact of the activation of p38 MAPKs is dependent not only on the stimulus but also on the cellular context. Thus, it is important to understand how an insult to the embryo may trigger activation of the p38 MAPKs and alter cell fate determination. The role of p38 MAPK signaling in mediating teratogen-induced abnormal development remains to be elucidated.

Hydroxyurea (HU), an antineoplastic drug commonly used to treat sickle cell anemia and myeloproliferative diseases, has been studied extensively as a model teratogen. The recommended therapeutic doses of HU are in the range of 15 mg/kg/

day for sickle cell anemia and 80 mg/kg once every 3 days for chronic myelogenous leukemia. HU is a potent DNA synthesis inhibitor; it directly inhibits ribonucleoside diphosphate reductase and hinders the reductive conversion of ribonucleotides to deoxyribonucleotides, resulting in rapid inhibition of DNA replication (Sneeden and Loeb, 2004). In mice, thymidine ^{3}H incorporation into DNA in the skin and thymus is decreased to 5% of control at 0.5 and 1 h after an ip injection of 100 mg/kg HU; DNA synthesis in the liver is reduced to 20–40% of control at this time (Smith *et al*., 1968). In rabbits, DNA synthesis in the embryos is reduced 10-fold 2 h after a sc injection of 650 mg/kg HU (DeSesso and Goeringer, 1990). During this replication stress, DNA is prone to breakage and the genome is unstable (Chan *et al*., 2009).

HU also induces the generation of reactive oxygen species (ROS). The hydroxylamine group in HU interacts with oxygen in biological tissues to produce the highly reactive hydroxyl radical and hydrogen peroxide (DeSesso, 1979). The production of ROS induces oxidative stress, adversely affecting cellular metabolism and leading to cell cycle arrest and cell death (DeSesso, 1979). Thus, HU induces both oxidative and replication stress, modifying macromolecules such as DNA, proteins, and lipids in the embryo. In previous studies, we have shown that *in utero* exposure to HU increases the formation of 4-hydroxynonenal protein adducts in embryos and induces caudal skeletal defects (Yan and Hales, 2006). Previous studies have also revealed that MAPK signaling is activated in HU-exposed organogenesis-stage mouse embryos; moreover, inhibition of p38 MAPK activation increases fetal death in HU-exposed embryos (Yan and Hales, 2008), demonstrating that p38 MAPK signaling plays an essential role in the survival of the conceptus after insult with this teratogen.

We hypothesize that HU exposure triggers oxidative stress, inducing p38 MAPK activation, and replication stress, inducing DNA damage response signaling, and that these responses are enhanced in the organogenesis-stage embryo in malformation-sensitive tissues. To test this hypothesis, we examined the temporal and spatial localization of the activation of MEK3/6 and p38 MAPK and the DNA damage response, as assessed by the formation of nuclear γH2AX foci, in HU-exposed embryos. We report that the HU-induced DNA damage response is ubiquitous; however, even in the presence of DNA damage, cell death was not increased in the heart, a relatively malformation-resistant organ. In contrast, activation of the p38 MAPK signaling pathway was region specific and enhanced in malformation-sensitive tissues of the embryo.

MATERIALS AND METHODS

Animals, treatments, and embryo collection. All animal protocols were approved by the Animal Care Committee of McGill University (protocol no. 1825) in conformance with the guidelines outlined in the Guide to the Care and Use of Experimental Animals, prepared by the Canadian Council on Animal Care.

Timed-pregnant CD1 mice were purchased from Charles River Canada Ltd (St Constant, QC, Canada) and housed at the McIntyre Animal Resource Centre (McGill University, Montreal, QC, Canada). Female virgin mice were mated between 8:00 a.m. and 10:00 a.m. on gestation day (GD) 0. On GD9, saline (control) or HU (Aldrich Chemical Co., Madison, WI; 400 or 600 mg/kg) was given to females by ip injection at 9:00 a.m. Dams were euthanized at 0.5, 3, or 6 h after treatment by CO_2 inhalation and cervical dislocation. The uteri were removed, and embryos were dissected out in Hanks' balanced salt solution (Invitrogen Canada Inc., Burlington, ON, Canada). At the time of collection on GD9, for each dosage group, 3–4 embryos from each litter were fixed in paraformaldehyde for immunofluorescence-staining experiments. The remaining embryos from two litters were pooled together, snap frozen in liquid nitrogen, and stored at −80°C until later use for Western blotting experiments.

Western blotting. Whole tissue lysates were prepared for MEK 3/6, phospho-MEK-3/6, p38 MAPK, and phospho-p38 MAPK determinations. Samples, consisting of 10–18 embryos each (pooled from two litters), were placed in 60–100 µl of radioimmunoprecipitation assay buffer (150mM NaCl, 1% Nonidet P-40, 0.5% deoxycholate, 0.1% SDS, and 50mM Tris, pH 7.5) containing 10 µl/ml protease inhibitor cocktail and 20 µl/ml phosphatase inhibitor mix (Active Motif Inc., Carlsbad, CA). The samples were homogenized with an ultrasonicator (Sonics and Materials Inc., Newtown, CT) and centrifuged at 10,000 × g for 10 min at 4°C. The supernatants were used for immunoblotting.

Total proteins from each sample were quantified using the spectrophotometric Bio-Rad Protein Assay (Bio-Rad Laboratories Ltd, Mississauga, ON, Canada). Proteins (15 µg from each sample) were separated with 10% SDS-PAGE and then transferred onto equilibrated polyvinylidene difluoride membranes (Amersham Biosciences, Buckinghamshire, UK). Membranes were blocked with 5% skim milk for 1 h at room temperature and then probed overnight at 4°C with primary antibodies against MEK 3/6 (1:500, catalog number sc-13069; Santa Cruz Biotechnology Inc., Santa Cruz, CA), phospho-MEK-3/6 (1:2000, catalog number sc-8407, Santa Cruz Biotechnology), p38 MAPK (1:1000, catalog number no. 9212, Cell Signaling Technology Inc., Danvers, MA), phospho-p38 MAPK (1:1000, catalog number no. 4511, Cell Signaling Technology), and β-actin (1:5000, catalog number sc-1616, Santa Cruz Biotechnology).

Membranes were incubated with horseradish peroxidase–conjugated secondary antibodies (1:10,000; GE Healthcare, Buckinghamshire, UK) for 2 h at room temperature, and proteins were detected by enhanced chemiluminescence (GE Healthcare). The bands were quantified by densitometric analysis using a ChemiImager 400 imaging system (Alpha Innotech, San Leandro, CA); the peak area represents the intensity of the band. Each experiment was replicated five to ten times with different pooled litters for each dosage group.

Immunofluorescence. At the times of collection on GD9, 3–4 embryos were collected from each litter and fixed for 4 h at 4°C in 4% paraformaldehyde. Embryos were then dehydrated in ethanol, embedded in paraffin, and serially sectioned (5 µm sections) along the sagittal plane. Tissue sections were deparaffinized and rehydrated with water. After rinsing twice for 2 min each with PBS, sections were subjected to antigen unmasking by incubating in sodium citrate buffer (10mM sodium citrate trisodium salt dehydrate, pH 6.0) and microwaving at 100% power for 2 min and then 10% power for 10 min. Slides were allowed to cool at room temperature for 15 min and then rinsed in PBS for 5 min.

Phospho-MEK-3/6 immunoreactivity was detected using a M.O.M immunodetection kit (Vector Laboratories, Burlington, CA) as follows. Sections were incubated in the working solution of M.O.M mouse IgG blocking reagent for 1 h in a humidified chamber. After further rinses with PBS, twice for 2 min each, sections were incubated in the working solution of M.O.M diluents for 5 min. Solution was gently tipped off the slides, and sections were then incubated for 30 min at room temperature with a mouse monoclonal anti-phospho-MEK-3/6 (Ser187/Ser209) (1:100, catalog number sc-8407, Santa Cruz Biotechnology Inc.) in M.O.M diluent. After washing twice for 2 min in PBS, the sections were incubated in the working solution of M.O.M biotinylated anti-mouse IgG reagent for 10 min, followed by washing twice for 2 min in PBS. The sections

were stained with Fluorescein Avidin DCS for 5 min, washed thrice for 5 min in PBS, mounted with Vectashield for fluorescence with DAPI mounting medium (Vector Laboratories), and covered with cover slips.

Phospho-p38 MAPK and γH2AX immunoreactivity were detected as follows. Sections were incubated in blocking serum (0.5% bovine serum albumin [BSA], 0.1% Triton X-100, 10% goat serum in PBS) for 1 h at room temperature in a humidified chamber. Serum was gently tipped off the slides, primary antibody against phospho-p38 MAPK (1:50; catalog number no. 4511, Cell Signaling Technology) and γH2AX (1:100; catalog number ab2893; Abcam, Cambridge, MA) were diluted in antibody diluent buffer (0.5% BSA, 0.1% Triton X-100, 1.5% goat serum in PBS), and sections were incubated overnight at 4°C or 1 h at room temperature, respectively. Sections were rinsed thrice for 5 min in PBS and then incubated with secondary goat anti-rabbit IgG (1:100, catalog number A11008, Invitrogen), diluted in antibody diluent buffer for 1 h at room temperature. After washing thrice for 5 min in PBS, sections were counterstained with propidium iodide (Sigma-Aldrich Co., St Louis, MO) at 10 µg/ml in antibody diluent buffer for 5 min at room temperature and then washed again with PBS, thrice for 5 min each. Finally, slides were mounted with Vectashield mounting medium (Vector Laboratories, Inc.) and covered with cover slips.

All slides were stored at 4°C and visualized with a fluorescence or confocal microscope within 2 days. As a negative control for phospho-MEK-3/6, phospho-p38 MAPK, and γH2AX staining, the primary antibodies were preadsorbed with phospho-MEK-3/6 blocking peptide (Santa Cruz Biotechnology, Inc), phospho-p38 MAPK blocking peptide (Cell Signaling Technology, Inc.), or γH2AX blocking peptide (Abcam Inc.), respectively.

Fluorescence and confocal microscopy. Phospho-MEK-3/6 immunoreactivity images were captured with a Leica DM LB2 fluorescence microscope (Leica Microsystems Inc., Concord, ON) using a 40× lens fitted with an Infinity-3 video camera (Lumenera Corp., Ottawa, ON).

Phospho-p38 MAPK and γH2AX immunoreactivities were visualized using a Zeiss LSM 510 Axiovert 100M confocal microscope with a Plan-Apochromat x63/1.4 oil DIC objective (Supplementary fig. S4). All embryos were scanned at a 1.65 µs pixel time speed with an optical slice of approximately 0.6 µm, zoom factor equal to 0.7, and a pinhole setting of 96 µm for phospho-p38 MAPK and γH2AX and 88 µm for propidium iodide. Z-stack images of five independent saline-treated and HU-treated embryos from each group were acquired.

Optimal settings for fluorescence imaging were determined experimentally for all primary antibodies and maintained for all embryos. For whole embryo images, stained embryos were carefully traced and captured at 20× magnification with the fluorescence microscope, and images were stitched together using the Microsoft Image Composite Editor software (Microsoft Corporation, Albuquerque, NM).

Quantitative analysis. For quantitative analysis of phospho-MEK-3/6, saline- and HU-treated embryos were analyzed using MetaMorph Image Analysis software (Molecular Devices, Sunnyvale, CA). Two regions of interest were randomly selected and created within an image by a 2D box of 200 × 200 µm. Then the intensity means were analyzed in the cropped images. The unit of measure (*N*) was the number of saline- or HU-treated pregnant females. For the control group, $N = 5$ females with 13, 14, and 13 embryos were analyzed in the 0.5, 3, and 6 h groups, respectively. For the low dose (400 mg/kg) HU-treated embryo groups, $N = 5$ females with 15, 14, and 15 embryos were analyzed at 0.5, 3, and 6 h, respectively. For the high dose (600 mg/kg) HU-treated embryo group, $N = 5$ females with 15, 14, and 14 embryos were analyzed at 0.5, 3, and 6 h, respectively (Supplementary table S1).

Measurements of phospho-p38 MAPK and γH2AX immunoreactivities were analyzed using Imaris Software (Bitplane AG, Zurich, Switzerland). For each image, two regions of interest were randomly selected and created by a 3D box of 50 × 50 × 14 µm. Three-dimensional iso-surfaces of saline- and HU-treated embryos were generated, and total intensity means were measured for the staining of phospho-p38 MAPK. For the quantification of nuclear staining, a nuclear surface was first created from propidium iodide staining for each image; within that surface, phospho-p38 MAPK and γH2AX were isolated. The nuclear intensity means were analyzed for phospho-p38 MAPK; γH2AX foci were quantified based on their volume normalized to the nuclear volume. An animation of the nuclear quantification is included in the Supplementary figure S1. For the analysis of phospho-p38 MAPK, the sample size for the control, low dose, and high dose groups was $N = 5$ females; 10 embryos were analyzed at each time point for each group (i.e., 2 embryos/female). For the analysis of γH2AX, the sample size for each dose group and time point was $N = 5$ females; 13–15 embryos were analyzed for each group at each time point (2–3 embryos per female) (Supplementary tables S2–S4).

Images from γH2AX staining were used to analyze pyknotic nuclei. Green channel (γH2AX) was turned off, and propidium iodide staining was isolated using IMARIS. The total numbers of nuclei and of pyknotic nuclei were counted in each image.

The five areas quantified for each embryo were the rostral neuroepithelium (RNE), caudal neuroepithelium (CNE), neural tube (NT), somite (S), and heart (H) (as indicated in Supplementary fig. S2). To compare the intensity means and DNA damage between the HU-treated groups and the control group, the values for the control group were set to 1, and the fold differences from control were examined. All the immunofluorescence analyses for this study are summarized in Supplementary tables S1–S4.

Statistical analyses. All statistical analyses were done by two-way ANOVA using GraphPad Prism version 5.00 (GraphPad Software, San Diego, CA). Dunnett's test was done to analyze the drug effect between control and HU-treated embryos. Tukey's multiple comparison test was used to assess any differences in the intensity means of phospho-MEK-3/6 and phospho-p38 MAPK, as well as γH2AX foci volume, among the five selected regions at 3 h in each treatment group. All values were reported as fold difference from the control group, set to 1 ± SEM. The *a priori* level of significance was $p < 0.05$.

RESULTS

HU Induced Widespread Activation of MEK-3/6 in GD9 Embryos

The expression of total and activated MEK-3/6 protein was determined in GD9 embryos 0.5, 3, and 6 h post-treatment with saline (C), low (L: 400 mg/kg), or high (H: 600 mg/kg) dose HU. Total MEK-3/6 protein concentrations were not altered by HU treatment at 0.5, 3, or 6 h compared with saline controls (Fig. 1A). However, HU exposure induced a dramatic increase in the activation of MEK-3/6 at 0.5, 3, and 6 h as detected by an increase in phospho-MEK-3/6 in Western blots (Fig. 1B). Therefore, *in utero* HU exposure triggered the activation of MEK 3/6.

The localization of activated MEK-3/6 in the embryo was assessed to determine the tissue specificity of the response to HU exposure. In saline-treated embryos, low amounts of phospho-MEK-3/6 immunoreactivity (green color) were detected in the embryos (Figs. 2A and B). Exposure to HU increased the activation of MEK-3/6 as demonstrated by an increase in fluorescence intensity. Phospho-MEK-3/6 immunoreactivity was widespread and enhanced in HU-exposed embryos; activated MEK-3/6 was detected in the rostral neuroepithelium (RNE), caudal neuroepithelium (CNE), neural tube (NT), somites (S), and heart (H) (Fig. 2B). Quantitative analysis of the fluorescence in these regions using MetaMorph revealed a dose-dependent increase in phospho-MEK-3/6 total intensity in HU-exposed embryos compared with control/saline-treated embryos (Fig. 3). At 3 h post-treatment, a threefold increase in reactivity was observed in the rostral and caudal neuroepithelium and heart in the high-dose HU group compared with the

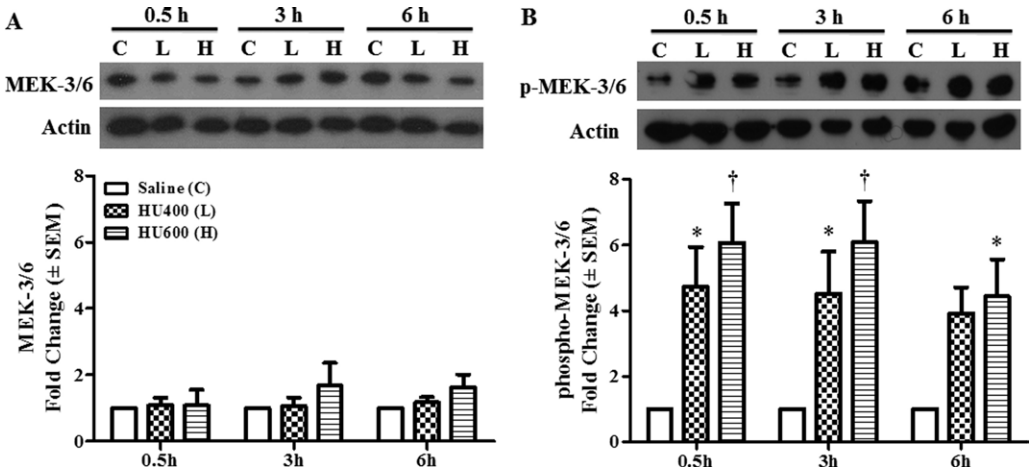

FIG. 1. HU induced activation of MEK-3/6. (A) Western blot analysis of total protein expression of MEK 3/6 at 0.5, 3, and 6 h after treatment with HU at 400 mg/kg (L) or 600 mg/kg (H) is shown in the upper panel. The lower panel shows the densitometry quantification of MEK 3/6. (B) Western blot analysis of phospho-MEK 3/6 at 0.5, 3, and 6 h after treatment with HU at 400 mg/kg (L) or 600 mg/kg (H) is shown in the upper panel. The lower panel shows the densitometry quantification of phospho-MEK 3/6. There was a dose-dependent increase in phospho-MEK-3/6 at all time points. Each bar (mean ± SEM) represents embryos from five sets of pooled litters with two litters per pool ($n = 5$). * and †, significantly different from saline (control) group at the same time point (*$p < 0.05$; †$p < 0.01$, Dunnett's test).

saline group (Fig. 3). To determine whether activated MEK-3/6 preferentially localized to a specific region within the embryo, Tukey's analysis was done to compare the five regions against each other within a treatment group (a total of 10 comparisons). There were no significant differences in phosho-MEK3/6 total mean intensities among the five regions in either the saline- or the HU-treated embryos (Fig. 3F and Supplementary fig. S3A). Therefore, HU treatment induced a widespread activation of MEK-3/6 in embryos.

HU Promoted Localized Activation and Nuclear Translocation of p38 MAPK

Because the upstream MEK3/6 kinases catalyze phosphorylation of the downstream p38 MAPKs, we determined the effects of HU exposure on the activation and localization of p38 MAPK. Western blot analysis showed that the total expression of p38 MAPK was not affected by HU treatment at 0.5, 3, or 6 h (Fig. 4A), but its activation was enhanced after exposure to increasing doses of HU (Fig. 4B). Exposure to high-dose HU significantly increased the phosphorylation of p38 MAPK at 3 h post-treatment compared with the saline group (Fig. 4B). The maximum amplitude of this increase (10.7-fold) exceeded that observed for phospho-MEK-3/6; the activation of p38 MAPK was transitory because by 6 h post-treatment HU-exposed embryos did not differ significantly from controls. Phospho-p38 MAPK immunofluorescence staining was distributed globally in control embryos (Fig. 5A, Supplementary fig. S3B); the total intensity increased with increasing HU dose (Figs. 5A and B). Similarly, Tukey's test was carried out to determine the region specificity of the distribution of phospho-p38 MAPK within the embryo. Contrary to the widespread MEK-3/6 activation observed in embryos, quantitative analysis of phospho-p38 MAPK immunoreactivity 3 h after HU treatment revealed that p38 MAPK was preferentially activated in the RNE, CNE, and NT of HU-treated embryos (Figs. 6A–C). Although there was also an increase in total phospho-p38-MAPK in the somite and heart (Figs. 6E and F), the mean changes were not significant. Activated p38 MAPKs phosphorylate substrates in the cytoplasm and nucleus. Therefore, our next goal was to determine whether HU exposure altered the intracellular distribution of phospho-p38 MAPK in embryos. We used confocal microscopy and IMARIS 3D imaging software surface rendering to assess phospho-p38 MAPK immunofluorescence in the cytosol and nucleus. This allowed the removal of cytosol staining, isolating the nuclear staining; cytosol and nuclear intensities were quantified separately (Supplementary fig. S1). In control embryos, phospho-p38 MAPK was detected primarily in the cytosol, with low amounts in the nucleus and no region specificity (Figs. 5A and B; Supplementary fig. S3C). Exposure to HU resulted in the nuclear accumulation of phospho-p38 MAPK (Figs. 5A, 5B, and 7). HU exposure significantly increased the nuclear intensity of phospho-p38 MAPK in the RNE, CNE, NT, and somite compared with the saline group (Fig. 7); peak amounts of nuclear phospho-p38 MAPK were observed in the neuroepithelium at 3 h. At this time, Tukey's analysis revealed that there was a significant region-specific nuclear accumulation of phospho-p38 MAPK in the RNE and CNE (Fig. 7F). Although total phospho-p38 MAPK was expressed highly in the neuroepithelium and NT (Fig. 6F), nuclear phospho-p38 MAPK was preferentially localized to the neuroepithelium (Fig. 7F). Because the total protein expression of p38 MAPK was unaffected by HU treatment (Fig. 4A), the increase in nuclear expression of

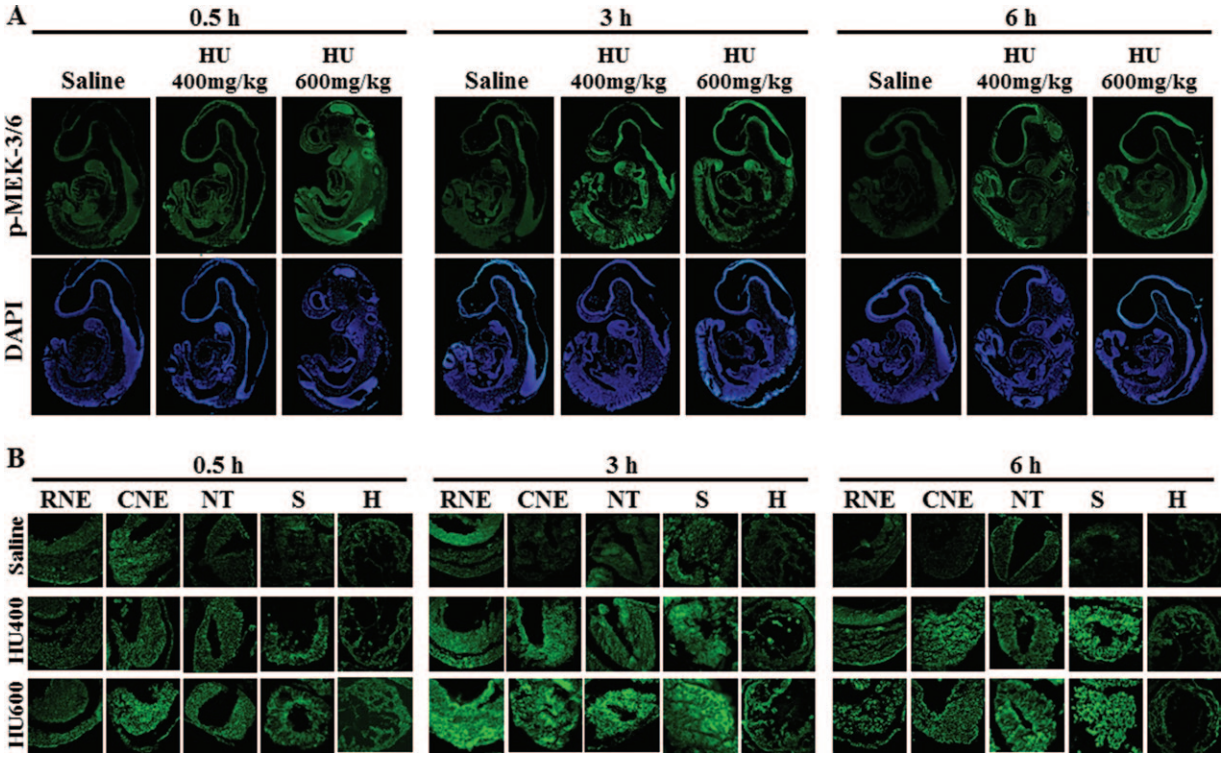

FIG. 2. The localization of activated MEK 3/6 in GD9 embryos exposed to HU. Timed-pregnant female mice received saline or HU at 400 or 600 mg/kg on GD9. Embryos were processed for immunofluorescence staining with an antibody against phospho-MEK-3/6 (in green) and counterstained with DAPI (in blue). (A) Whole embryo views of phospho-MEK-3/6 immunoreactivity at 0.5, 3, and 6 h post-HU treatment. (B) 40× magnification of the selected five regions in an embryo: rostral neuroepithelium (RNE), caudal neuroepithelium (CNE), neural tube (NT), somite (S), and heart (H).

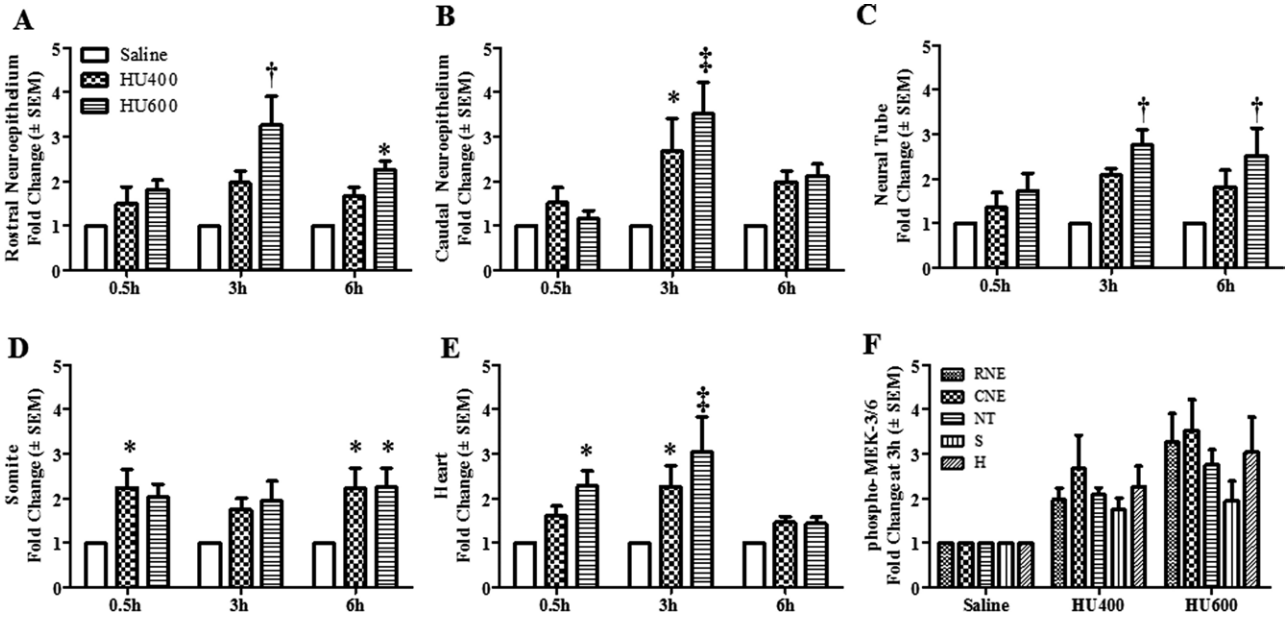

FIG. 3. Intensity means of phospho-MEK-3/6 in different regions of GD9 embryos. The quantification of phospho-MEK-3/6 immunoreactivity by intensity mean in GD9 embryos exposed to saline or HU at 400 or 600 mg/kg in different regions is presented in the RNE (A), CNE (B), NT (C), somite (D), and heart (E). Values were normalized to the corresponding saline control and expressed as fold changes. $n = 5$. Asterisks, daggers, and double daggers denote a significant difference from saline control at the same time point (*$p < 0.05$; †$p < 0.01$; ‡$p < 0.001$, Dunnett's test). (F) Phospho-MEK-3/6 staining at 3 h post-HU treatment. There were no significant regional differences in phospho-MEK-3/6 staining within the embryo.

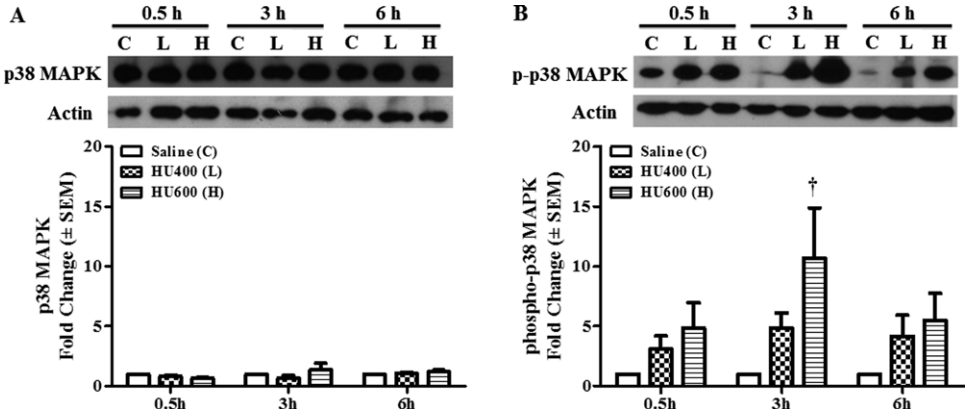

FIG. 4. HU induced activation of p38 MAPK. (A) Western blot analysis of total protein expression of p38 MAPK at 0.5, 3, and 6 h after treatment with HU at 400 mg/kg (L) or 600 mg/kg (H) is shown in the upper panel; the lower panel depicts the scan densitometry quantification of p38 MAPK. (B) Western blot analysis of phosphorylated p38 MAPK at 0.5, 3, and 6 h after treatment with HU at 400 mg/kg (L) or 600 mg/kg (H) is shown in the upper panel; the lower panel depicts the scan densitometry quantification of phospho-p38 MAPK. Phospho-p38 MAPK expression was significantly different from control in embryos 3 h after treatment with HU at 600 mg/kg. Each bar (mean ± SEM) represents embryos from six sets of pooled litters, with two litters per pool. *, significantly different from saline (control) group at the same time point (†$p < 0.01$, Dunnett's test).

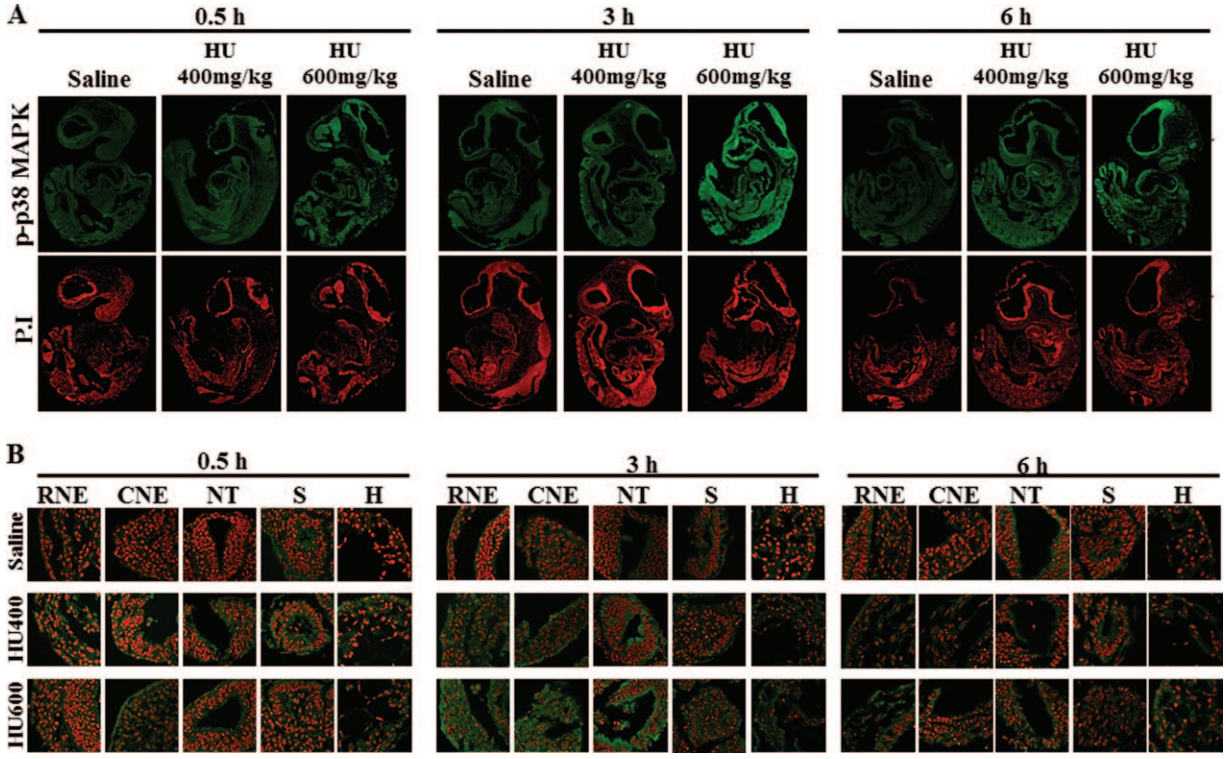

FIG. 5. The localization of phospho-p38 MAPK in GD9 embryos exposed to HU. Timed-pregnant female mice received saline or HU at 400 or 600 mg/kg on GD9. Embryos were processed for immunofluorescence staining with an antibody against phospho-p38 MAPK (in green) and counterstained with propidium iodide (in red). (A) Whole embryo views of phospho-p38 MAPK immunoreactivity at 0.5, 3, and 6 h posttreatment. (B) 60× magnification views of the selected five regions in an embryo: RNE, CNE, NT, somite (S), and heart (H).

phospho-p38 MAPK was due to protein translocation rather than the translation of new protein. Thus, these results suggest that p38 MAPK is activated dramatically in response to HU insult; moreover, phospho-p38 MAPK is translocated into the nucleus in a region-specific manner within the embryo.

HU Induced Localized DNA Damage and Altered Nuclear Morphology

Because DNA damage inducing stimuli trigger the nuclear translocation of phospho-p38 MAPK, we investigated the impact of HU treatment on DNA damage in embryos using γH2AX as a

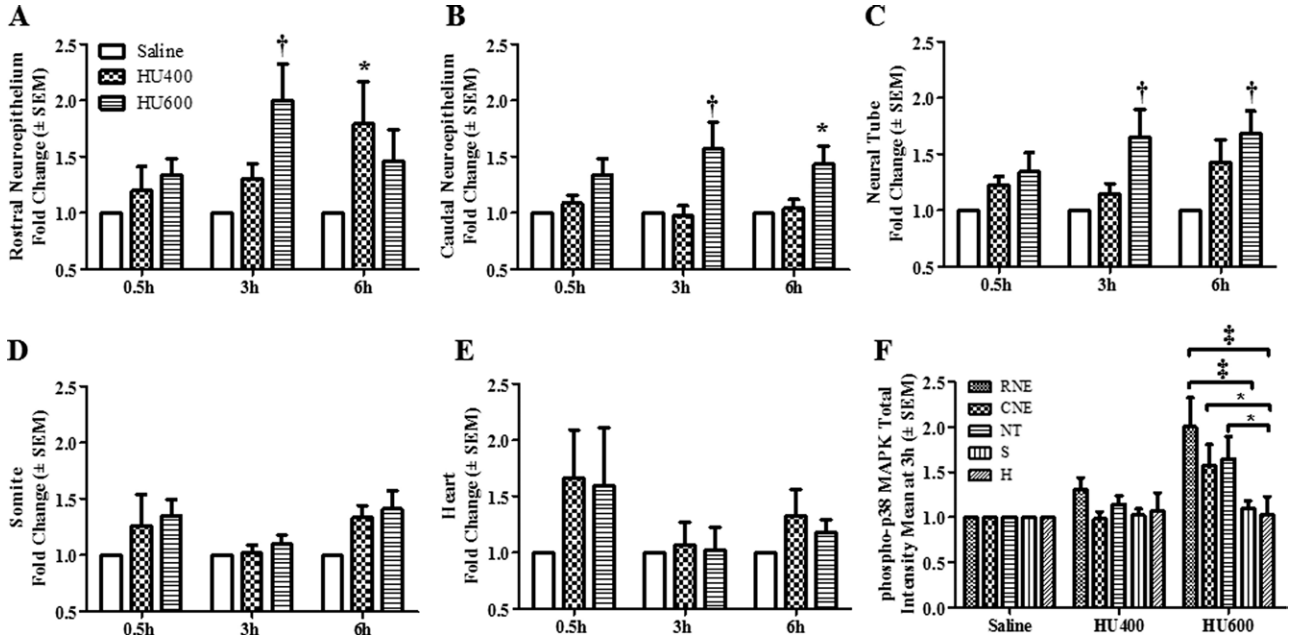

FIG. 6. Total intensity means of phospho-p38 MAPK in different regions of GD9 embryos. The quantification of total phospho-p38 MAPK immunoreactivity by intensity means in GD9 embryos exposed to saline or HU at 400 or 600 mg/kg in different regions is presented for the RNE (A), CNE (B), NT (C), somite (D), and heart (E). Values were normalized to the corresponding saline control and expressed as fold changes. $n = 5$. Asterisks, daggers, and double daggers denote a significant difference from saline control at the same time point (*$p < 0.05$; †$p < 0.01$; ‡$p < 0.001$, Dunnett's test). (F) Regional differences in total phospho-p38 MAPK reactivity in control and HU-exposed embryos. At 3 h posttreatment, RNE was significantly different than somite and heart (‡$p < 0.001$); CNE and NT were both significantly different than heart (*$p < 0.05$, Tukey's multiple comparison test).

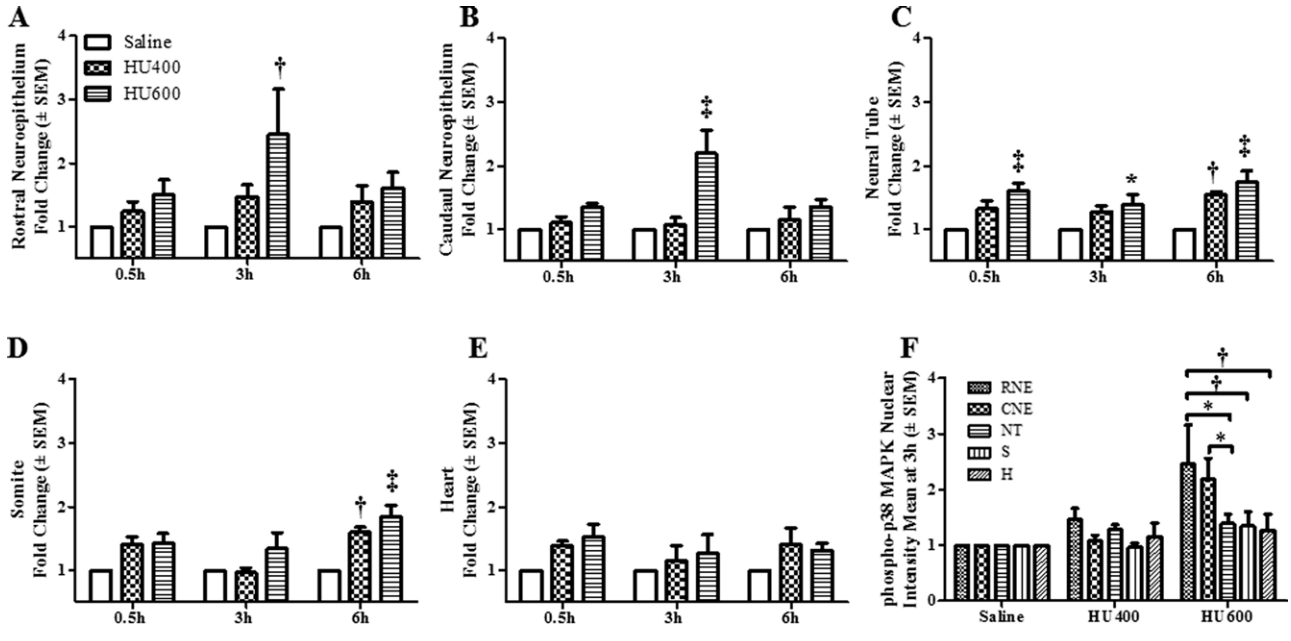

FIG. 7. Nuclear intensity means of phospho-p38 MAPK in different regions of GD9 embryos. The quantification of nuclear phospho-p38 MAPK immunoreactivity by intensity mean in GD9 embryos exposed to saline or HU at 400 or 600mg/kg in different regions is presented for the RNE (A), CNE (B), NT (C), somite (D), and heart (E). Values were normalized to the corresponding saline control and expressed as fold changes. $n = 5$. Asterisks, daggers, and double daggers denote a significant difference from saline control at the same time point (*$p < 0.05$; †$p < 0.01$; ‡$p < 0.001$, Dunnett's test). Panel (F) illustrates the regional differences in nuclear phospho-p38 MAPK expression found in RNE and CNE of embryos exposed to HU at 600 mg/kg. RNE was significantly different than NT (*$p < 0.05$), somite, and heart (†$p < 0.01$); CNE was significantly different than heart (*$p < 0.05$, Tukey's multiple comparison test).

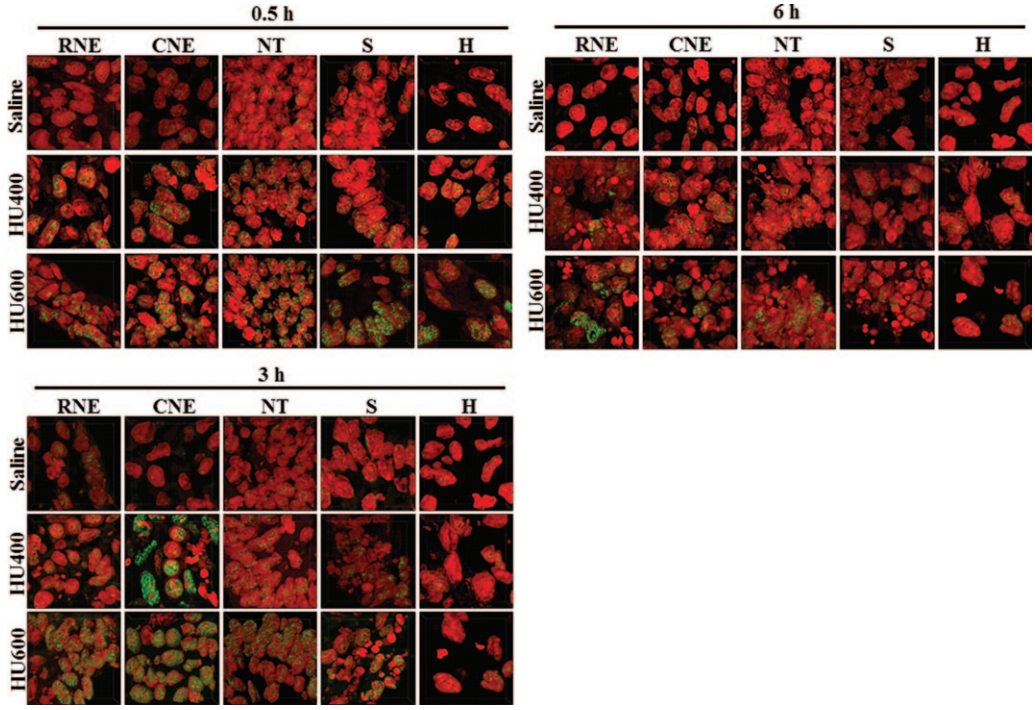

FIG. 8. γH2AX staining in GD9 embryos exposed to HU. The detection of DNA DSBs with γH2AX in saline and HU-exposed embryos in different regions. Immunodetection of γH2AX is in green and nuclear propidium iodide in red. Images display quantification regions (50 × 50 × 14 μm), which were randomly selected from each structure taken at 63× magnification (shown in Supplementary fig. S4).

marker for DNA double-strand breaks (DSBs). Low numbers of γH2AX foci were observed in all regions of the control embryos (Fig. 8; Supplementary fig. S3D). HU-treated embryos exhibited a dramatic increase in the overall γH2AX signal intensities and in the numbers of γH2AX foci compared with the saline-treated embryos (Fig. 8). The foci in the high-dose HU (HU600) group were so concentrated that they appeared as clusters within the nuclei. Therefore, γH2AX focal volume was chosen as the parameter to be measured quantitatively. Comparisons of the mean volumes of γH2AX foci indicated that a significant increase occurred in the HU-treated embryos in each of the five regions (Fig. 9). Temporally, this increase occurred as early as 0.5 h (NT) post-HU treatment; the response peaked at 3 h in all tissues. Spatially, the greatest increase in γH2AX focal volumes within the embryos was observed in the CNE, with up to a 13.5-fold increase compared with the saline-treated group. A comparison among the five regions indicated a significant difference in γH2AX focal volumes in the CNE of the embryos exposed to high-dose HU (Fig. 9). Thus, the HU-induced activation of DNA damage signaling pathways in the embryo during organogenesis was enhanced in this malformation-sensitive tissue.

The nuclei of cells that are in the process of dying, by apoptosis or necrosis, display an irreversible condensation of chromatin known as pyknosis. The propidium iodide staining of the nuclei of saline-treated and HU-exposed embryos was detected in cells in the process of dying. Embryos exposed to saline showed normal nuclear morphology at all time points. However, pyknotic nuclei and cell fragmentation were observed in HU-treated embryos starting at 3 h posttreatment (Fig. 10). The numbers of pyknotic nuclei were increased in all affected regions at 6 h, reaching up to 41% (Fig. 10). It is interesting to note that pyknotic nuclei were observed in all regions of the embryo except the heart even though γH2AX foci were increased significantly in the heart (Fig. 9).

DISCUSSION

Maternal exposure to HU activated p38 MAPK and its upstream mediator, MEK3/6, in the organogenesis-stage embryo. MEK 3/6 is crucial in mediating the activation of p38 MAPK. Studies have shown that MEK3/6 double knockout mice die during embryogenesis due to a placental defect (Mudgett *et al.*, 2000), whereas mice deficient only in MEK 3 or MEK6 are viable but display a decrease in long bone mineralization and p38 MAPK activation (Greenblatt *et al.*, 2010). Thus, the MEK3/6-p38 MAPK axis is a major mediator of skeletal mineralization. Both MEK3/6 and p38 MAPK were activated in embryos 0.5 h post-HU treatment, at a time when previous studies have shown that HU induces oxidative stress (Yan and Hales, 2006). This association suggests that free radical species may be one of the stimuli that triggers p38 MAPK signaling. Similarly, γH2AX foci formation is observed as early as 0.5 h post-HU treatment, suggesting that free radicals may directly attack DNA and cause strand breaks. Moreover, this

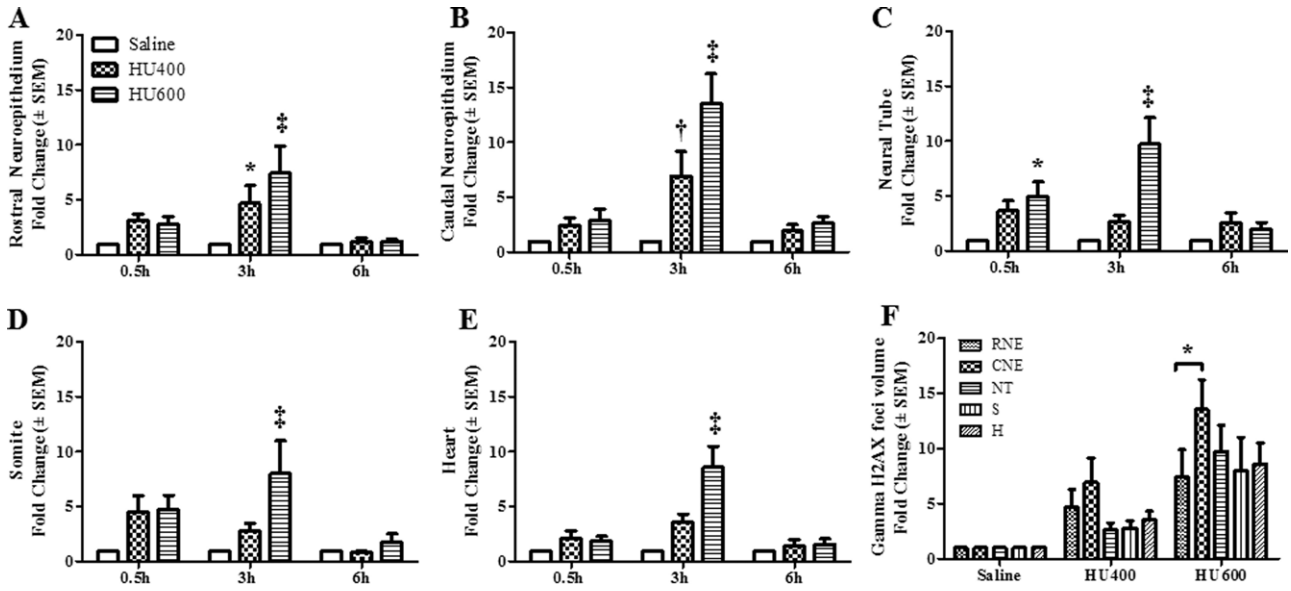

FIG. 9. γH2AX focal volumes in different regions of GD9 embryos. The quantification of γH2AX focal volumes in different regions of the GD9 embryos exposed to saline or HU at 400 or 600 mg/kg is presented for the RNE (A), CNE (B), NT (C), somite (D), and heart (E). Values were normalized to the corresponding saline controls and expressed as fold changes. $n = 5$. Asterisks, daggers, and double daggers denote a significant difference from saline controls at the same time point (*$p < 0.05$; †$p < 0.01$; ‡$p < 0.001$, Dunnett's test). (F) The regional differences in γH2AX focal volumes found in the CNE of embryos exposed to HU at 600 mg/kg. CNE was significantly different than RNE (*$p < 0.05$, Tukey's multiple comparison test).

direct free radical–induced damage to DNA may induce DNA damage signals, which, in turn, activate the p38 MAPK pathway. Both the formation of γH2AX foci and the activation of p38 MAPK peaked at 3 h post-HU treatment. We anticipate that DNA synthesis is still reduced at this time after HU treatment (DeSesso and Goeringer, 1990; Smith *et al*., 1968). Stalled replication forks lead to replication stress and further induce DNA strand breaks (Feng *et al*., 2011). Thus, HU-mediated embryotoxicity may be due to two mechanisms, oxidative stress and replication stress.

Interestingly, the localization of activated kinases in embryos was more region specific for phospho-p38 MAPK, the downstream target kinase, than for MEK-3/6. MEK-3/6 activation was widespread in the embryo, whereas p38 MAPK activation was localized to the RNE, CNE, and NT. Phospho-p38 MAPK was found predominantly in the cytoplasm in control embryos. Upon HU exposure, preferential translocation of phospho-p38 MAPK into the nucleus was observed in the RNE and CNE. This nuclear translocation may be a specific response to stimuli that induce DNA DSBs, whereas other exposures, such as to sodium arsenite, promote the cytoplasmic accumulation of phospho-p38 MAPK (Ben-Levy *et al*., 1998). The HU-induced nuclear accumulation of phospho-p38 MAPK will enable the activation of its nuclear substrates, such as MAPKAP kinase-2 (MK2) and p53, both of which induce cell cycle checkpoints and facilitate DNA repair (Bulavin *et al*., 2001). Activation of cell cycle checkpoints in response to DNA damage is essential for the maintenance of genomic stability. Reinhardt and colleagues (2007) have shown that downregulation of MK2 caused regression of tumour cells *in vivo*, leading to mitotic catastrophe after treatment with DNA damaging agents (Reinhardt *et al*., 2007). Because previous studies have shown that the inhibition of p38 MAPK enhanced fetal mortality after HU exposure (Yan and Hales, 2008), we propose that p38 plays a role in protecting the embryo from HU insult. Furthermore, the disruption of the p38 MAPK-MK2 axis may increase the sensitivity of embryos to HU by disrupting normal checkpoint functions and allowing cells with damaged DNA strands to enter mitosis, leading to mitotic catastrophe and resulting in an increase in apoptotic cell death. Therefore, in addition to its well-described role in apoptosis, p38 MAPK may also be important in mediating survival in embryos.

Caudal regions of the embryo are of special interest to us because caudal defects predominate in embryos exposed to HU on GD9. In this study, we report that the CNE displayed the highest accumulation of phospho-p38 MAPK and γH2AX foci in the nuclei. HU-induced damage in the caudal region of the embryo may exceed the repair capacity of cells in this area, leading to the induction of apoptosis as indicated by the increase in pyknotic nuclei observed 6 h post-HU treatment. Interestingly, the heart was the only region in which an increase in pyknotic nuclei was not observed. Cells in the heart have a longer cell cycle; the presence of fewer cells in S phase would be expected to result in fewer pyknotic nuclei after HU exposure. The heart is also an organ that is resistant to insult by a number of cytotoxic teratogens (Mirkes and Little, 1998). HU-induced nuclear phospho-p38 MAPK was relatively low in the heart. During limb development, p38 MAPK was activated where cell death occurs in the interdigital tissue. Moreover, nuclear labeling of phospho-p38 MAPK increased during tissue regression, suggesting

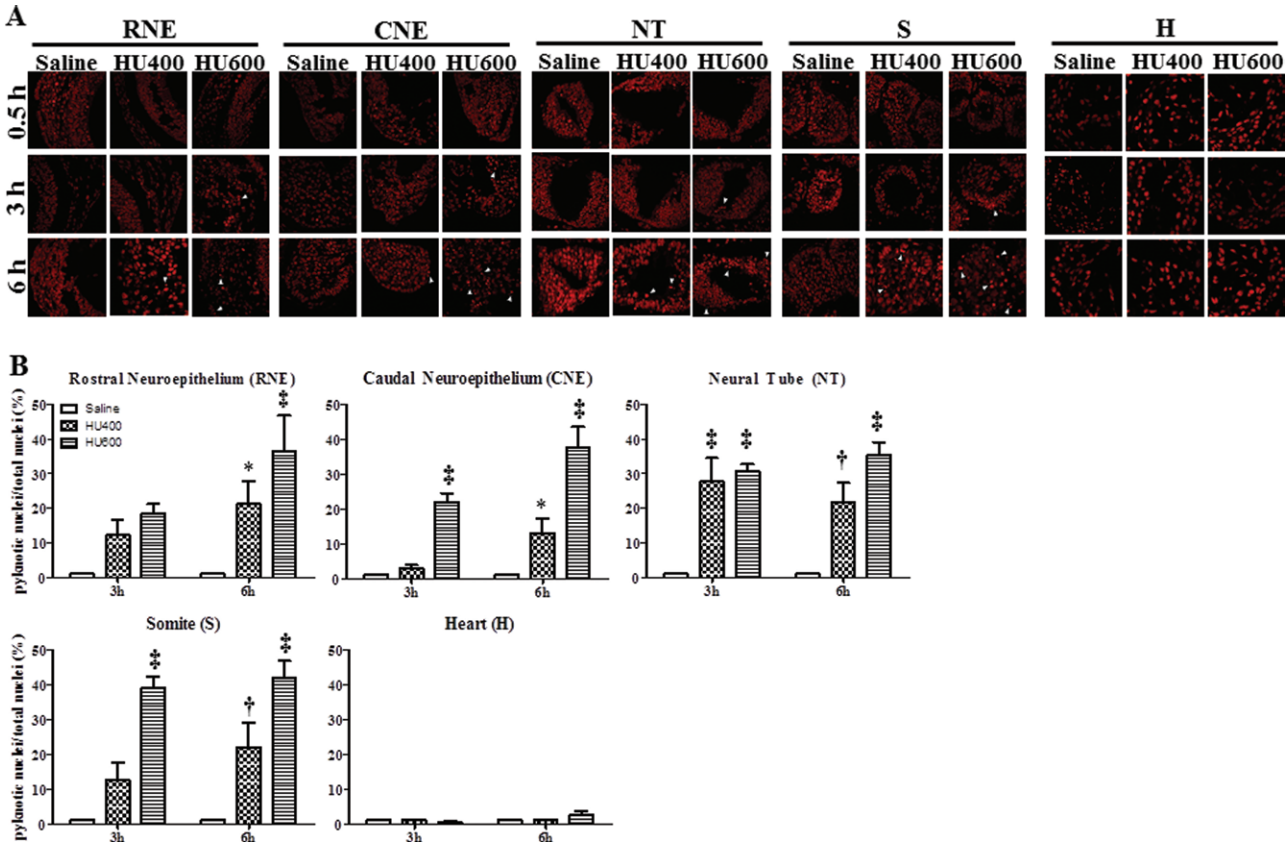

FIG. 10. Pyknotic nuclei in different regions of the GD9 embryos exposed to HU. (A) Propidium iodide staining of the RNE, CNE, NT, somite (S), and heart (H) in saline and HU-exposed embryos at 0.5, 3, and 6 h posttreatment. The arrowheads indicate pyknotic nuclei. (B) Quantification of pyknotic nuclei by IMARIS. Each bar (mean ± SEM) represents the percentage of pyknotic nuclei. Embryos from five litters per treatment group were analyzed. Asterisks, dagger, and double dagger denote a significant difference from saline control at the same time point (*$p < 0.05$; †$p < 0.01$; ‡$p < 0.001$, Dunnett's test).

that p38 MAPK mediates the upregulation of genes involved in programmed cell death (Zuzarte-Luís *et al*., 2004). Because the absence of cell death in the heart is accompanied by low levels of nuclear phospho-p38 MAPK, the expression of cell death genes regulated by p38 MAPK may be repressed in the heart.

The absence of cell death despite the formation of γH2AX foci in the embryonic heart may also suggest that there is sufficient DNA repair to preserve chromatin architecture and, ultimately, cell survival in this organ. Immediate and efficient repair after the induction of DNA DSBs is important to restore and preserve the integrity and functionality of chromatin. Phosphorylation of H2AX is a key step in the DNA damage response, playing a role in signaling and initiating the repair of DNA DSBs (Celeste *et al*., 2002). The formation of γH2AX foci represents an epigenetic signal that helps in the recruitment and accumulation of DNA damage response proteins at the sites of DNA strand breaks (Kinner *et al*., 2008). In parallel, p38 MAPK modulates the cell cycle checkpoint response, providing the time required for DNA repair. Interestingly, this appears to be true only at relatively low levels of DNA damage (Kinner *et al*., 2008). After higher levels of damage, extensive chromosome breakage results in cells that are incapable of resuming DNA synthesis (Feng *et al*., 2009). Because the formation of γH2AX foci is low in the heart compared with the CNE, we predict that DNA damage in the heart is below a critical threshold, allowing this damage to be sufficiently repaired for cells to survive. In addition, it has been proposed that the cytoplasmic accumulation of p38 MAPK favors a survival response. Reinhardt *et al*. (2010) discovered a late cell cycle checkpoint that is controlled by cytoplasmic p38 MAPK. It is possible that sustained cell cycle arrest is occurring in the heart, allowing this organ to undergo more efficient DNA repair.

The increases in activation of the p38 MAPK signaling and DNA damage response pathways as a result of HU-induced oxidative and replication stress suggest that these pathways may serve as intracellular effectors of the embryonic stress response. It is clear that the regulation of p38 MAPK signaling is complex. Further insight into the identification of p38 MAPK nuclear substrates in different regions of the embryo is a priority in understanding the decision of cells to execute different pathways, i.e., apoptosis in the CNE versus cell survival and differentiation in the heart. In addition, the extent to which a teratogenic insult stimulates the DNA repair process in the embryo remains to be determined.

SUPPLEMENTARY DATA

Supplementary data are available online at http://toxsci.oxfordjournals.org/.

FUNDING

Canadian Institutes of Health and Research (FRN-57867). S.B. received funding from FRQS. B.F.H. is the recipient of a James McGill Professorship.

ACKNOWLEDGMENTS

Image processing and analysis for this article were performed in the McGill University Life Sciences Complex Imaging Facility. We thank the Imaging Facility Team, Aleksandrs Spurmanis and Claire Brown (McGill University, Montreal), for their diligent efforts and guidance in using the IMARIS software and Jacynthe Laliberte (McGill University, Montreal) for her assistance with confocal microscopy.

REFERENCES

Ben-Levy, R., Hooper, S., Wilson, R., Paterson, H. F., and Marshall, C. J. (1998). Nuclear export of the stress-activated protein kinase p38 mediated by its substrate MAPKAP kinase-2. *Curr. Biol*. **8,** 1049–1057.

Bradham, C. A., and McClay, D. R. (2006). p38 MAPK is essential for secondary axis specification and patterning in sea urchin embryos. *Development* **133,** 21–32.

Bulavin, D. V., Higashimoto, Y., Popoff, I. J., Gaarde, W. A., Basrur, V., Potapova, O., Appella, E., and Fornace, A. J., Jr. (2001). Initiation of a G2/M checkpoint after ultraviolet radiation requires p38 kinase. *Nature* **411,** 102–107.

Celeste, A., Petersen, S., Romanienko, P. J., Fernandez-Capetillo, O., Chen, H. T., Sedelnikova, O. A., Reina-San-Martin, B., Coppola, V., Meffre, E., Difilippantonio, M. J., *et al.* (2002). Genomic instability in mice lacking histone H2AX. *Science* **296,** 922–927.

Chan, K. L., Palmai-Pallag, T., Ying, S., and Hickson, I. D. (2009). Replication stress induces sister-chromatid bridging at fragile site loci in mitosis. *Nat. Cell Biol*. **11,** 753–760.

Cuadrado, A., and Nebreda, A. R. (2010). Mechanisms and functions of p38 MAPK signalling. *Biochem. J*. **429,** 403–417.

Deacon, K., Mistry, P., Chernoff, J., Blank, J. L., and Patel, R. (2003). p38 Mitogen-activated protein kinase mediates cell death and p21-activated kinase mediates cell survival during chemotherapeutic drug-induced mitotic arrest. *Mol. Biol. Cell* **14,** 2071–2087.

DeSesso, J. M. (1979). Cell death and free radicals: A mechanism for hydroxyurea teratogenesis. *Med. Hypotheses* **5,** 937–951.

DeSesso, J. M., and Goeringer, G. C. (1990). The nature of the embryo-protective interaction of propyl gallate with hydroxyurea. *Reprod. Toxicol*. **4,** 145–152.

Enslen, H., Brancho, D. M., and Davis, R. J. (2000). Molecular determinants that mediate selective activation of p38 MAP kinase isoforms. *EMBO J*. **19,** 1301–1311.

Feng, W., Bachant, J., Collingwood, D., Raghuraman, M. K., and Brewer, B. J. (2009). Centromere replication timing determines different forms of genomic instability in Saccharomyces cerevisiae checkpoint mutants during replication stress. *Genetics* **183,** 1249–1260.

Feng, W., Di Rienzi, S. C., Raghuraman, M. K., and Brewer, B. J. (2011). Replication stress-induced chromosome breakage is correlated with replication fork progression and is preceded by single-stranded DNA formation. *G3 (Bethesda)*. **1,** 327–335.

Greenblatt, M. B., Shim, J. H., Zou, W., Sitara, D., Schweitzer, M., Hu, D., Lotinun, S., Sano, Y., Baron, R., Park, J. M., *et al.* (2010). The p38 MAPK pathway is essential for skeletogenesis and bone homeostasis in mice. *J. Clin. Invest*. **120,** 2457–2473.

Kinner, A., Wu, W., Staudt, C., and Iliakis, G. (2008). Gamma-H2AX in recognition and signaling of DNA double-strand breaks in the context of chromatin. *Nucleic Acids Res*. **36,** 5678–5694.

Kurosu, T., Takahashi, Y., Fukuda, T., Koyama, T., Miki, T., and Miura, O. (2005). p38 MAP kinase plays a role in G2 checkpoint activation and inhibits apoptosis of human B cell lymphoma cells treated with etoposide. *Apoptosis* **10,** 1111–1120.

Mirkes, P. E., and Little, S. A. (1998). Teratogen-induced cell death in postimplantation mouse embryos: Differential tissue sensitivity and hallmarks of apoptosis. *Cell Death Differ*. **5,** 592–600.

Mudgett, J. S., Ding, J., Guh-Siesel, L., Chartrain, N. A., Yang, L., Gopal, S., and Shen, M. M. (2000). Essential role for p38alpha mitogen-activated protein kinase in placental angiogenesis. *Proc. Natl. Acad. Sci. U.S.A*. **97,** 10454–10459.

Puri, P. L., Wu, Z., Zhang, P., Wood, L. D., Bhakta, K. S., Han, J., Feramisco, J. R., Karin, M., and Wang, J. Y. (2000). Induction of terminal differentiation by constitutive activation of p38 MAP kinase in human rhabdomyosarcoma cells. *Genes Dev*. **14,** 574–584.

Reinhardt, H. C., Aslanian, A. S., Lees, J. A., and Yaffe, M. B. (2007). p53-deficient cells rely on ATM- and ATR-mediated checkpoint signaling through the p38MAPK/MK2 pathway for survival after DNA damage. *Cancer Cell* **11,** 175–189.

Reinhardt, H. C., Hasskamp, P., Schmedding, I., Morandell, S., van Vugt, M. A., Wang, X., Linding, R., Ong, S. E., Weaver, D., Carr, S. A., *et al.* (2010). DNA damage activates a spatially distinct late cytoplasmic cell-cycle checkpoint network controlled by MK2-mediated RNA stabilization. *Mol. Cell* **40,** 34–49.

She, Q. B., Chen, N., and Dong, Z. (2000). ERKs and p38 kinase phosphorylate p53 protein at serine 15 in response to UV radiation. *J. Biol. Chem*. **275,** 20444–20449.

Smith, H. C., Boutwell, R. K., and Potter, V. R. (1968). Effects of hydroxyurea on DNA and RNA synthesis in mouse skin, liver, and thymus and on skin tumorigenesis initiated by beta-propiolactone. *Cancer Res*. **28,** 2217–2227.

Sneeden, J. L., and Loeb, L. A. (2004). Mutations in the R2 subunit of ribonucleotide reductase that confer resistance to hydroxyurea. *J. Biol. Chem*. **279,** 40723–40728.

Suzanne, M., Irie, K., Glise, B., Agnès, F., Mori, E., Matsumoto, K., and Noselli, S. (1999). The Drosophila p38 MAPK pathway is required during oogenesis for egg asymmetric development. *Genes Dev*. **13,** 1464–1474.

Tamura, K., Sudo, T., Senftleben, U., Dadak, A. M., Johnson, R., and Karin, M. (2000). Requirement for p38alpha in erythropoietin expression: A role for stress kinases in erythropoiesis. *Cell* **102,** 221–231.

Uhlik, M. T., Abell, A. N., Johnson, N. L., Sun, W., Cuevas, B. D., Lobel-Rice, K. E., Horne, E. A., Dell'Acqua, M. L., and Johnson, G. L. (2003). Rac-MEKK3-MKK3 scaffolding for p38 MAPK activation during hyperosmotic shock. *Nat. Cell Biol*. **5,** 1104–1110.

Wood, C. D., Thornton, T. M., Sabio, G., Davis, R. A., and Rincon, M. (2009). Nuclear localization of p38 MAPK in response to DNA damage. *Int. J. Biol. Sci*. **5,** 428–437.

Yan, J., and Hales, B. F. (2006). Depletion of glutathione induces 4-hydroxynonenal protein adducts and hydroxyurea teratogenicity in the organogenesis stage mouse embryo. *J. Pharmacol. Exp. Ther*. **319,** 613–621.

Yan, J., and Hales, B. F. (2008). p38 and c-Jun N-terminal kinase mitogen-activated protein kinase signaling pathways play distinct roles in the response of organogenesis-stage embryos to a teratogen. *J. Pharmacol. Exp. Ther*. **326,** 764–772.

Zuzarte-Luís, V., Montero, J. A., Rodriguez-León, J., Merino, R., Rodríguez-Rey, J. C., and Hurlé, J. M. (2004). A new role for BMP5 during limb development acting through the synergic activation of Smad and MAPK pathways. *Dev. Biol*. **272,** 39–52.